Fischer–Tropsch Synthesis: Assessment of the Ripening of Cobalt Clusters and Mixing between Co and Ru Promoter via Oxidation–Reduction-Cycles over Lower Co-Loaded Ru–Co/Al2O3 Catal...

ARTICLE *in* INDUSTRIAL & ENGINEERING CHEMISTRY RESEARCH · DECEMBER 2007

Impact Factor: 2.59 · DOI: 10.1021/ie0709988

6 AUTHORS, INCLUDING:

Amitava Sarkar
TOTAL
29 PUBLICATIONS **194** CITATIONS
SEE PROFILE

Mingsheng_(Mason) LUO
Beijing Institute of Petrochemical Technology
21 PUBLICATIONS **417** CITATIONS
SEE PROFILE

Alan K Dozier
NIOSH/DART
42 PUBLICATIONS **1,151** CITATIONS
SEE PROFILE

Burtron Davis
University of Kentucky
604 PUBLICATIONS **10,930** CITATIONS
SEE PROFILE

Fischer−Tropsch Synthesis: Assessment of the Ripening of Cobalt Clusters and Mixing between Co and Ru Promoter via Oxidation−Reduction-Cycles over Lower Co-Loaded Ru−Co/Al_2O_3 Catalysts

Gary Jacobs,[†] Amitava Sarkar,[†] Yaying Ji,[†] Mingsheng Luo,[†] Alan Dozier,[‡] and Burtron H. Davis*[,†]

Center for Applied Energy Research, University of Kentucky, 2540 Research Park Drive, Lexington, Kentucky 40511, and University of Kentucky Electron Microscopy Center, Chemical and Materials Engineering Department, A004 ASTeCC Building 0286, Lexington, Kentucky 40506

A 2% Ru-promoted 15% Co/Al_2O_3 catalyst was tested after reduction and after being subjected to oxidation−reduction cycles. The catalysts were characterized over four oxidation−reduction cycles by XANES/EXAFS, TPR, HRTEM, and EDS elemental mapping. The oxidation−reduction treatments were found to assist in sintering the metallic clusters to a larger size, and to promote mixing on at least the order of the nanoscale. The larger crystallites in closer proximity to the Ru promoter led to a more facile reduction of the cobalt crystallites. In addition, a catalyst exposed to two oxidation−reduction cycles resulted in slightly higher conversion, higher α-value product, slightly lower methane selectivity, and greater stability over a reduced freshly calcined catalyst.

1. Introduction

Fischer−Tropsch synthesis (FTS) is normally carried out with either a cobalt- or iron-based catalyst depending on the ratio of H_2/CO in the feed. As a step in gas-to-liquids (GTL) technology, cobalt catalysts are often preferred[1,2] due to the low intrinsic water gas shift (WGS) activity of cobalt. While in many typical supported-metal catalysts a low metal loading is preferable for obtaining a high surface area of available active metal, the same is not the case with cobalt/alumina FTS catalysts, a commercial catalyst for slurry-based GTL operations. Commercial catalysts are, in fact, heavily loaded with cobalt, and companies have reported ratios up to 30 g of Co to 100 g of alumina.[1,2] This is an impressive number, considering that many supported-metal reforming catalysts contain only 0.005−1% of highly dispersed metal. One reason for the high loadings is due to the strong interaction of small cobalt oxide species with the alumina support. Increasing the cobalt cluster size weakens the interaction, allowing a greater fraction of the active cobalt metal to reduce. Compare the hydrogen chemisorption/pulse reoxidation data in Table 1 for the 15% and 25% Co loadings for catalyst reduced at 350 °C for 10 h, which is a common reduction condition for Fischer−Tropsch synthesis catalysts. The 25% Co catalyst exhibits 42% reduction versus 30% for the 15% Co catalyst, but the average diameter is larger (11.8 nm versus 5.9 nm for the 15% Co loading). The reduction of cobalt oxides on alumina follows primarily a two step reduction process from Co_3O_4 to CoO, and from CoO to Co metal.[3] While the first reduction step is quite facile, occurring at ∼350 °C, it is the second step which depends strongly on the interaction with the support. It would be beneficial to develop active catalysts with lower cobalt loadings, and one way to accomplish this is to facilitate reduction of the smaller and more strongly interacting cobalt oxide species by promoting the catalyst with a reduction promoter, such as Pt, Ru, or Re. As shown in Table 1, addition of a small amount of Pt to the low loading 15% Co catalyst doubles the extent of cobalt reduction while maintaining a small cluster size.[3]

While these catalysts do exhibit impressive initial activity, unfortunately, they deactivate quite rapidly compared to the more heavily cobalt-loaded commercial catalysts. The smaller clusters on the lower Co-loaded catalysts appear to be more prone to sintering,[4−7] and in water co-feeding studies,[8−13] they have been suggested to be more sensitive than the more heavily loaded cobalt catalysts to support-induced reoxidation phenomena, which likely involve cobalt−support complex formation.[8,9,11−16] These deactivation processes appear to be cluster size (and, therefore, support) sensitive. Some researchers have chosen to explore the preparation of cobalt catalysts with much weaker support interactions (e.g., silica[17−19] or carbon nanotubes[20]) to benefit from high reducibility. However, here we have taken a different course and opted to try to improve cobalt/alumina catalysts, as the support interaction appears to be important for the stabilization of a small cluster size. Furthermore, alumina benefits as a support for being attrition resistant, a property that is key for slurry phase FT processes.

Therefore, in this work, the aim is to develop a better working cobalt/alumina catalyst with a low cobalt loading (∼15% Co). The goal is to maintain the presence of a reduction promoter in the catalyst to assist in the reduction of the smaller, more highly interacting cobalt oxide species. Yet at the same time, the interest is to use pretreatments to essentially grow the cobalt cluster to a suitable size that is more resistant to cluster-size-related deactivation phenomena. Oxidation−reduction cycles have in the past proven fruitful for accelerating the aging (i.e., sintering) of metal particles, and this technique was chosen for ripening the cobalt clusters. One additional benefit of the method may be improved mixing between the active metal and the promoter.[21]

In this investigation, 2% Ru−15% Co/Al_2O_3 was prepared by a wet impregnation technique. Oxidation−reduction cycles were performed on the material, and the impacts on resulting cluster size, extent of reduction, degree of promoter interaction, and catalytic behavior were assessed.

2. Experimental Section

2.1. Catalyst Preparation and Oxidation−Reduction Cycle Pretreatments. A large batch of 2% Ru−15% Co/Al_2O_3 catalyst

[†] Center for Applied Energy Research.
[‡] University of Kentucky Electron Microscopy Center.

10.1021/ie0709988 CCC: $40.75
Published on Web 12/20/2007

Table 1. Influence of Loading and Promoter Addition on Size and Percent Reduction[3]

catalyst	H_2 desorbed (μmol/g)	uncorrected % dispersion	uncorrected diam (nm)	% reduction	corrected % dispersion	corrected diam (nm)
15% Co/Al_2O_3	66.9	5.3	19.6	30	17.5	5.89
25% Co/Al_2O_3	77.7	3.7	28.2	42	8.7	11.8
0.5% Pt−15% Co/Al_2O_3	141	11.0	9.30	60	18.4	5.60

was prepared by a wet impregnation method using cobalt nitrate and ruthenium nitrosyl nitrate as precursors. The cobalt was added first, with vacuum drying in a rotary evaporator, and the ruthenium added second. The catalyst was calcined in air flow at 350 °C for 4 h. A batch of catalyst was removed (denoted freshly calcined catalyst), and the remaining catalyst was reduced in H_2:Ar (1:2) mixture at 350 °C for 5 h. The catalyst was cooled to room temperature in the H_2:Ar mixture, purged in argon, and then passivated using 1% O_2:He. A batch of catalyst was removed (RP#1 for reduced−passivated #1). The remaining catalyst was reintroduced to the reactor, and again calcined, reduced for 5 h, cooled, and passivated. Batch RP#2 was removed, and the process was carried out two more times to yield RP#3 and RP#4. However, for RP#3 and RP#4, the additional reduction cycles lasted 10 h.

2.2. Temperature Programmed Reduction (TPR). For TPR studies, the fresh catalyst and calcined (air flow, 350 °C) catalysts of RP#1, RP#2, RP#3, and RP#4 were evaluated to study the impact of the pretreatments on catalyst reducibility. The profiles were recorded using a Zeton-Altamira AMI-200 unit which makes use of a thermal conductivity detector (TCD). The samples were first ramped to 350 °C in pure Ar to drive off any residual H_2O from the sample, prior to cooling to 50 °C to begin the TPR. The tests were performed using a 10% H_2/Ar mixture referenced to Ar at a flow rate of 30 cm^3/min. The samples were heated to 800 °C at a ramp rate of 10 °C/min.

2.3. Extended X-ray Absorption Fine Structure (EXAFS)/ X-ray Absorption Near-Edge Spectroscopy (XANES). Samples RP#1−RP#4 were also evaluated by XANES and EXAFS spectroscopy at Brookhaven National Laboratory. Catalysts were re-reduced in the in situ flow cell in flowing H_2 at 350 °C and held for 30 min, prior to cooling to liquid nitrogen temperatures in flowing H_2. EXAFS/XANES spectra were taken in transmission mode at the National Synchrotron Light Source at Brookhaven National Laboratory, Upton, NY, Beamline X-18b. The beamline was equipped with a Si(111) channel cut monochromator. A crystal detuning procedure was used to help remove harmonic content from the beam and make the relative response of the incident and transmission detectors more linear. The X-ray flux for the beamline was on the order of 1×10^{10} photons per second at 100 mA and 2.8 GeV, and the usable energy range at X-18b is from 5.8 to 40 keV. EXAFS/XANES spectra were recorded near the Co and Ru K-edges. The spectra were recorded near the boiling temperature of liquid nitrogen to minimize contributions to the dynamic Debye−Waller factor. Sample thickness was determined by calculating the amount in grams per square centimeter of sample, w_D, by utilizing the following thickness equation:

$$w_D = \ln(I_o/I_t)/\sum\{(m/r)_j w_j\}$$

where m/r is the total cross section (absorption coefficient/ density) of element "j" in the sample at the absorption edge of the EXAFS element under study in cm^2/g, w_j is the weight fraction of element j in the sample, and $\ln(I_o/I_t)$ was taken over a typical range of 1−2.5. An average value of w_D from inputting both values was employed. Based on the calculation for w_D, and the cross-sectional area of the pellet, the grams were calculated. For example, at the Ru K-edge, the mass was typically ∼235 mg, and at the Co K-edge, the mass was ∼35 mg. Boron nitride was utilized in many cases to dilute the sample, such that the wafer could be self-supported. Smooth self-supporting pellets, free of pinholes, were pressed and loaded into the in situ XAS flow cell, and the treatment gas was directed to the sample area. The cell was purged for a long duration of time with a high flow rate of inert gas to ensure removal of air, prior to the re-reduction treatment.

EXAFS data reduction and fitting were carried out using the WinXAS,[22] Atoms,[23] FEFF,[24] and FEFFIT[24] programs. The k- and r-ranges were typically chosen to be 3−15 $Å^{-1}$ and 1.3−3.1 Å for the case of Co K-edge data, while the ranges were 5−16 $Å^{-1}$ and 1.9−2.7 Å for the case of Ru K-edge data. Details of the analysis procedures are reported elsewhere.[12]

For each XANES analysis, a linear combination of reference spectra was used to fit the data using the WinXAS[22] software.

2.4. High-Resolution Transmission Electron Spectroscopy/ Energy Dispersive X-ray Analysis. Resulting morphology and chemical composition of the catalysts prepared by oxidation−reduction cycles were analyzed by using a field emission analytical transmission electron microscope (JEOL JEM-2010F) operated at an accelerating voltage of 200 kV and equipped with a scanning transmission electron microscope (STEM) unit with a high-angle annular dark field (HAADF) detector, and a Gatan imaging filter (GIF)/PEELS system. HRTEM and energy dispersive X-ray spectroscopy (EDS) images were recorded under optimal focus condition at a typical magnification of 100K−500K. The electron beam had a point-to-point resolution of 0.5 nm. Gatan Digital Micrograph software was used for image and EELS data recording and processing.

The passivated catalyst samples were dissolved in *o*-xylene to form a slightly turbid suspension for use in high-resolution transmission electron microscopy (HRTEM). A drop of the suspension was placed with a syringe onto a lacey carbon film on 200 mesh copper grid. After the *o*-xylene evaporated, the grid was loaded into the microscope for analysis.

2.5. Reaction Testing in a CSTR. The freshly calcined catalyst and catalyst RP#3 were selected for performance testing in a CSTR. Polywax 3000 (polyethylene fraction with average molecular weight of 3000) purchased from Baker Petrolite, Inc., was used as start-up solvent. About 10−12 g of catalyst was reduced in a fixed bed reactor under flowing hydrogen for 10 h at 350 °C. The temperature during the reduction treatment was raised slowly from room temperature to 350 °C with a ramp rate of 1 °C/min. At the end of the activation period, the reactor was cooled to room temperature under hydrogen flow. The reduced catalyst was transferred to the CSTR that contained 310 g of Polywax 3000 pneumatically using ultrahigh purity nitrogen, and then re-reduced in situ at 250 °C for 24 h with a H_2 flow rate of 5 sl/h/g of catalyst (sl, standard liters).

The FTS experiments were conducted in a 1 L CSTR equipped with a magnetically driven stirrer with turbine impeller, a gas-inlet line, and a vapor outlet line with a stainless steel (SS) fritted filter (2 μm) placed external to the reactor. A tube fitted with a SS fritted filter (0.5 μm opening) extending below the liquid level of the reactor was used for withdrawing reactor

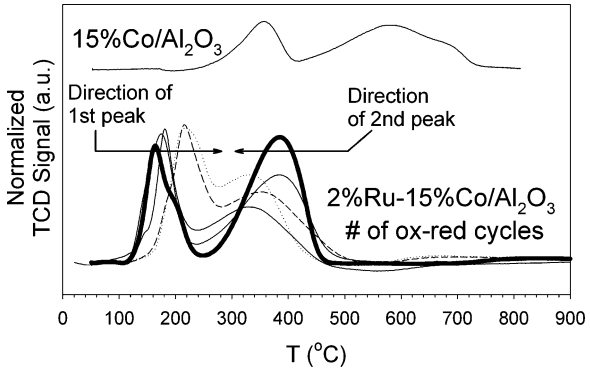

Figure 1. TPR profiles of 15% Co/Al_2O_3 and 2% Ru−15% Co/Al_2O_3 catalysts after a series of oxidation−reduction cycles.

wax (i.e., rewax, which is solid at room temperature), thereby maintaining a constant liquid level in the reactor. Another SS dip tube (1/8 in. outside diameter) extending to the bottom of the reactor was used to withdraw catalyst/wax slurry from the reactor at different times on-stream during synthesis. Separate mass flow controllers were used to control the flow of hydrogen and carbon monoxide at the desired rate. The gases were premixed in a mixing vessel before entering the reactor. Carbon monoxide was passed through a vessel containing lead oxide−alumina to remove any traces of iron carbonyl. The mixed gases entered the CSTR below the stirrer operated at 750 rpm. The reactor temperature was maintained constant (±1 °C) by a temperature controller.

The catalyst, reduced externally in a fixed bed reactor, was transferred pneumatically to the CSTR containing melted Polywax 3000 (at 150 °C) and reduced in situ for another 24 h. At the end of the in situ reduction period, FTS was started with a syngas space velocity (SV) of 8 sl/h/g of catalyst and the reactor temperature was slowly raised to 220 °C with a ramp rate of 0.5 °C/min. The H_2/CO ratio in syngas was maintained at 2.0. When the reactor temperature reached 220 °C, reactor pressure was slowly increased to 280 psig. Finally, the space velocity of the syngas was adjusted to obtain a CO conversion in the range 55−60%.

The conversions of CO and H_2 were obtained by gas-chromatographic analysis (micro-GC equipped with thermal conductivity detectors) of the product gas mixture. The reaction products were collected in three traps maintained at different temperatures: a hot trap (200 °C), a warm trap (100 °C), and a cold trap (0 °C). The products were separated into different fractions (wax, oil, and an aqueous phase) for quantification. For example, the oil product from the warm and cold traps were combined prior to GC analysis.

Table 2. Results of Linear Combination XANES Fitting: Co Component

catalyst	% CoO	% Co^0
2% Ru−15% Co/Al_2O_3, RP#1	95.0	5.0
2% Ru−15% Co/Al_2O_3, RP#2	58.6	41.4
2% Ru−15% Co/Al_2O_3, RP#3	47.2	52.8
2% Ru−15% Co/Al_2O_3, RP#4	35.9	64.1

3. Results and Discussion

TPR profiles are reported in Figure 1. The arrows indicate starting from the freshly calcined catalyst and moving toward a greater number of oxidation−reduction cycles. It is clear that, relative to unpromoted 15% Co/Al_2O_3, which completely reduces only at ∼800 °C, there is a shift in the reduction temperatures of both steps (i.e., Co_3O_4 to CoO and CoO to Co^0) to much lower temperatures (∼150−200 °C shift) with addition of the Ru promoter. The oxidation−reduction cycles led to a shift to higher temperature for the first reduction step, but, more importantly, to a decrease in the required temperature for the second step. To better understand the degree of catalyst reduction for both the Co and Ru components, XANES was utilized.

Figure 2 (left) displays the reference compounds for Co^0 and CoO, the two states present after the catalyst is reduced. Figure 2 (center) shows that little Co^0 was present after the first 5 h reduction treatment. However, with additional oxidation−reduction cycles, the cobalt systematically becomes more reduced. The spectra were fitted by taking a linear combination of the Co^0 and CoO references, and a sample fitting is provided in Figure 2 (right). The increasing extent of catalyst reduction is quantified in Table 2.

Interestingly, the Ru promoter is in a completely reduced state in all cases. The promoting effect of Ru may be an electronic influence due to alloying or, more likely, by providing sites for the dissociation and spillover of hydrogen, which can aid in nucleating the formation of reduced sites on the cobalt oxide species. The XANES results (Figure 3) are in agreement with the shifts observed by TPR.

EXAFS spectra of Co reference spectra are reported in Figure 4, while data for the 2% Ru−15% Co/Al_2O_3 catalyst are reported for the RP#1−RP#4 treatments (i.e., increasing number of oxidation−reduction cycles) in Figures 5 and 6. It is evident from XANES that, after the first reduction of 5 h, a large fraction of Co is CoO. With increasing oxidation−reduction cycles, the Fourier transform (FT) magnitude peaks (Figure 5) for Co−O and Co−Co in the CoO fraction decrease significantly, while the FT magnitude peak for Co−Co coordination in the Co^0 metal fraction increases, consistent with ripening.

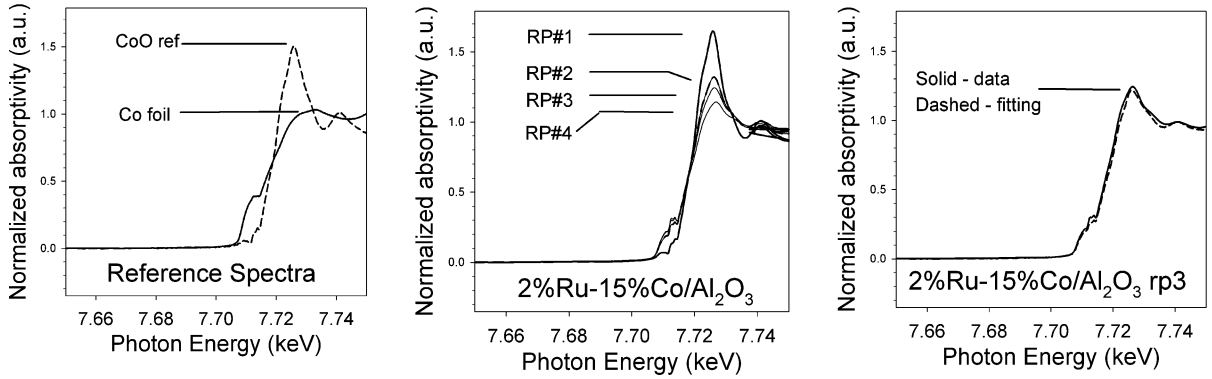

Figure 2. XANES profiles at the Co K-edge of (left) Co reference compounds, (center) 2% Ru−15% Co/Al_2O_3 catalysts after the oxidation−reduction cycle treatments, and (right) sample linear combination XANES fitting.

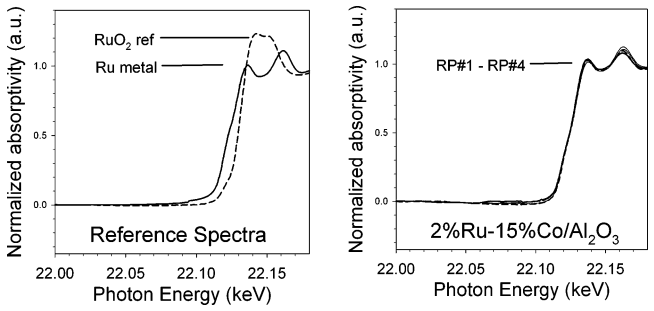

Figure 3. XANES profiles at the Ru K-edge of (left) reference compounds and (right) 2% Ru−15% Co/Al_2O_3 RP#1−RP#4 catalysts. The spectra virtually overlap.

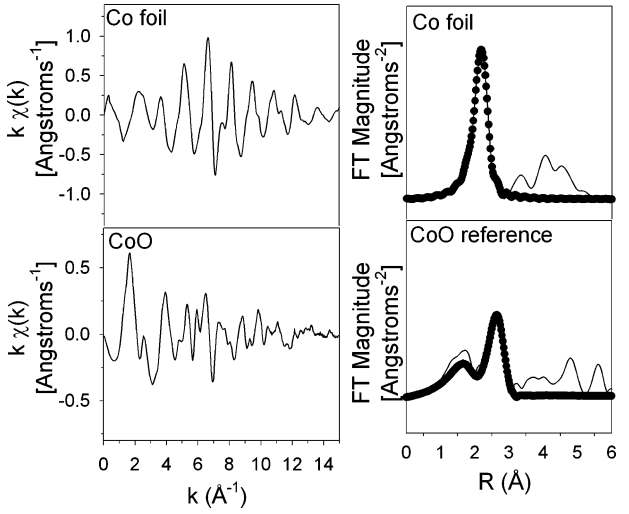

Figure 4. EXAFS results at the Co K-edge for the Co metal foil and CoO reference compounds, including filtering of the first Co−Co coordination shell and fitting.

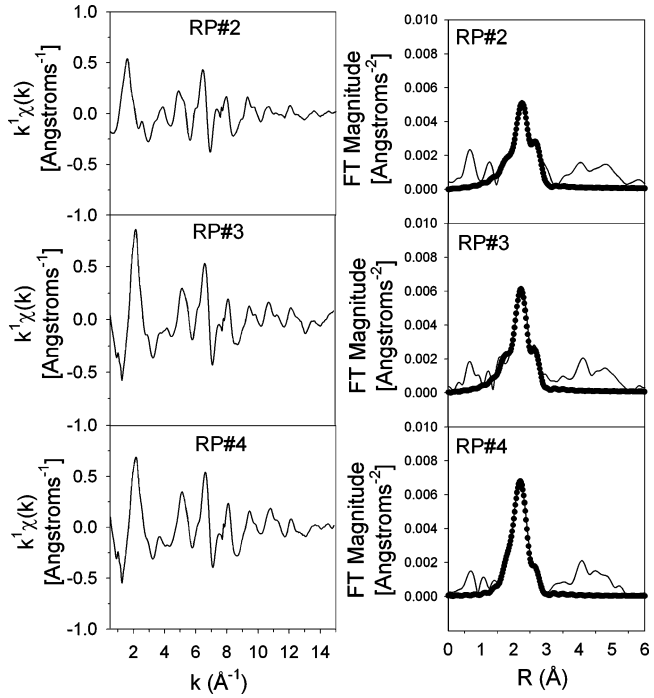

Figure 5. EXAFS results at the Co K-edge for the 2% Ru−15% Co/Al_2O_3 catalyst after reducing at 350 °C for 30 min of samples RP#1−RP#4. Note growth in Co−Co (metal) FT peak, consistent with a larger average Co cluster size, and a decrease in FT peaks for the oxide.

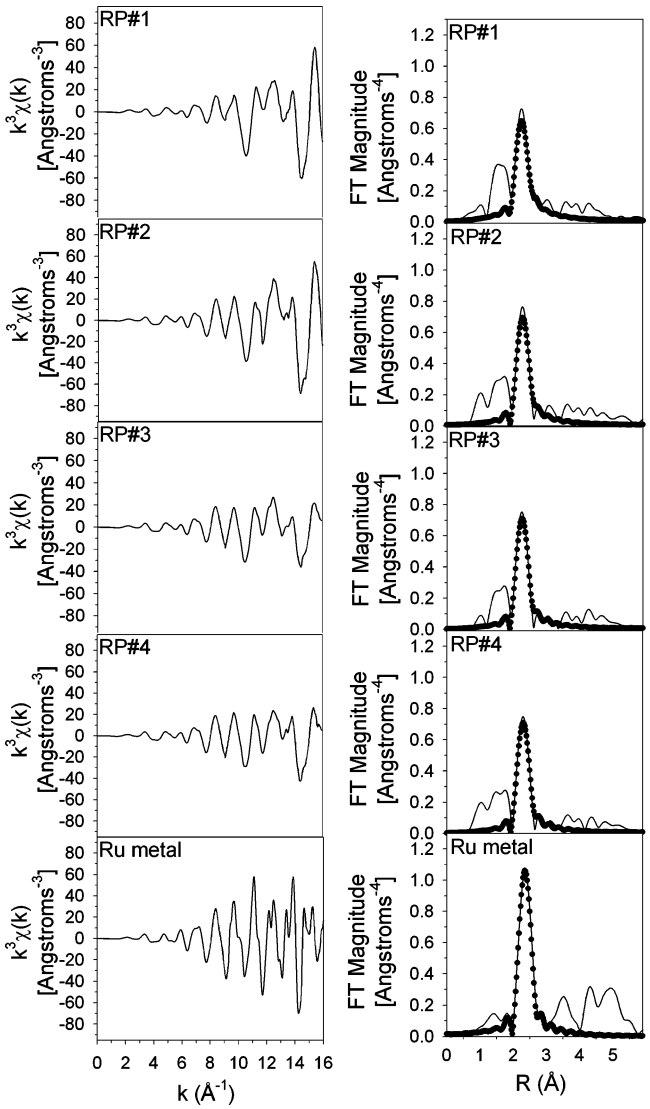

Figure 6. EXAFS results at the Ru K-edge for the 2% Ru−15% Co/Al_2O_3 catalyst after reducing at 350 °C for 30 min of samples RP#1−RP#4. Note growth in Ru−Ru (metal) FT peak, consistent with an increase in Ru crystallite size.

The EXAFS spectra for Ru indicate a Fourier transform magnitude peak for Ru−Ru coordination in the metal, which increases slightly with the number of oxidation−reduction cycles, as shown in Figure 6.

Results of EXAFS fittings are provided in Table 3. For cobalt, both first shell Co−O and Co−Co interactions (i.e., in the metal and in the CoO oxide) are included, while for Ru, only the first shell Ru−Ru interaction was fitted. Again, the tabulated EXAFS results of the fittings indicate that the degree of Co−Co coordination in the metal increases, while the degree of Co−O and Co−Co coordination in the oxide decreases (Table 3a). EXAFS and XANES results indicate that the average cobalt metal cluster size is increasing with the number of oxidation−reduction cycles and that, in addition to the influence of the Ru promoter, with a resulting increase in the cluster size the catalysts exhibit an enhanced extent of reduction due to a weakening of the Co−support interfacial interaction. The Ru promoter also displays an increase in Ru−Ru coordination number as a function of the number of oxidation−reduction cycles, suggesting some degree of cluster growth (Table 3b). We did not observe strong peaks indicating a Co−Ru interaction at the atomic level by EXAFS. However, it is important to

Table 3. Results of EXAFS Fitting for Data Acquired (a) Near the Co K Edge and (b) Near the Ru K Edge

(a) Results of EXAFS Fitting for Data Acquired Near the Co K Edge[a]

Co edge	n(Co−O)	R(Co−O) (Å)	n(Co−Co) metal	R(Co−Co metal) (Å)	n(Co−Co oxide)	R(Co−Co oxide) (Å)	e_0 (eV)	σ^2 (Å^2)	r-factor
Co foil			12.0 (set)	2.499 (0.0006)			7.65 (0.24)	0.00273 (0.00017)	0.0012
CoO	6.0 (set)	2.136 (0.003)			12.0 (set)	3.0163 (0.0032)	6.71 (0.72) 4.74 (1.09)	0.0159 (0.0019) 0.00762 (0.00054)	0.0190
CoRP#2	1.53 (0.30)	2.090 (0.032)	4.50 (0.64)	2.5064 (0.0045)	2.53 (0.56)	3.0165 (0.0067)	10.6 (1.78) 8.95 (1.78)	0.00378 (0.00115)	0.0123
CoRP#3	1.47 (0.32)	2.069 (0.026)	4.88 (0.66)	2.5029 (0.0041)	1.87 (0.55)	3.0061 (0.0084)	8.84 (1.70) 5.97 (2.18)	0.00294 (0.00105)	0.0165
CoRP#4	0.86 (0.21)	2.093 (0.037)	5.95 (0.47)	2.5008 (0.0025)	1.03 (0.40)	3.0134 (0.0111)	7.61 (1.08) 11.39 (2.59)	0.00340 (0.00063)	0.0040

(b) Results of EXAFS Fitting for Data Acquired Near the Ru K Edge[b]

Ru edge	n(Ru−Ru)	R(Ru−Ru) (Å)	e_0 (eV)	σ^2 (Å^2)	r-factor
Ru foil	12.0 (set)	2.6870 (0.0021)	−1.43 (2.23)	0.00261 (0.000507)	0.0076
RP#1	3.24	2.6617 (0.0020)	−9.10 (2.73)	−0.0324 (0.00199)	0.0056
RP#2	5.33	2.6634 (0.0023)	−7.56 (2.79)	−0.0307 (0.00227)	0.0078
RP#3	6.25	2.6679 (0.0024)	−5.08 (2.81)	−0.0262 (0.00239)	0.0088
RP#4	6.61	2.6683 (0.0019)	−4.05 (2.18)	−0.0258 (0.00189)	0.0055

[a] $S_0^2 = 0.789$ and $\Delta S_0^2 = 0.017$. [b] $S_0^2 = 0.889$ and $\Delta S_0^2 = 0.130$.

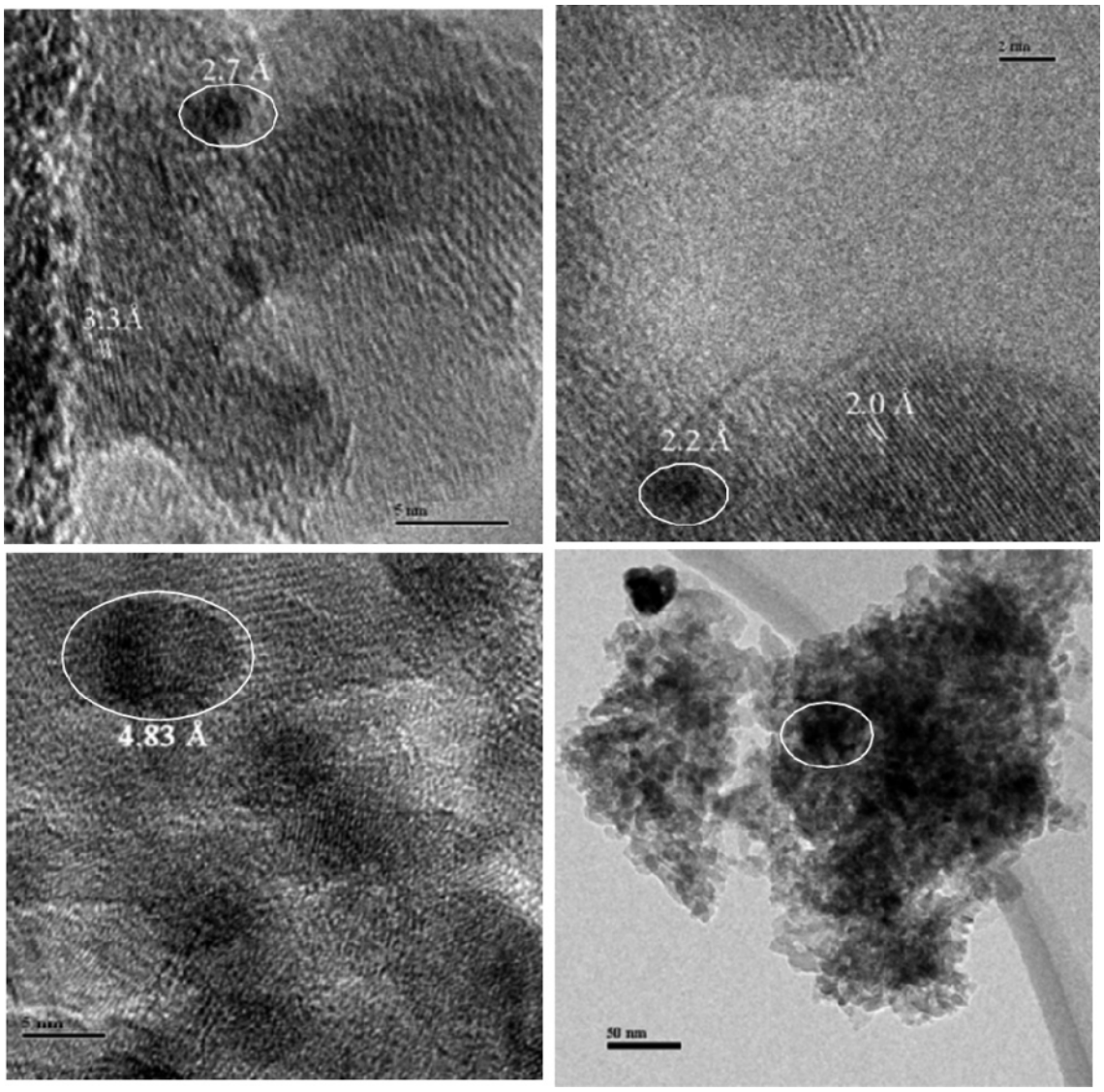

Figure 7. HRTEM images. (top left) Catalyst RP#1: crystalline structure with a characteristic *d*-spacing of 3.3 C is evident, while the dark area reveals a *d*-spacing of 2.7 C. (top right) RP#1 (duplicate): crystalline structure with a characteristic *d*-spacing of 2.0 C is observed, while the dark area reveals a *d*-spacing of 2.2 C. (bottom left) Catalyst RP#3: well-mixed crystalline nanoclusters with an average diameter of 5−10 nm can be found. (bottom right) Catalyst RP#4: well-mixed crystalline nanoclusters with an average diameter of about 20 nm are identified.

consider that, at lower promoter loadings, we have previously obtained evidence for Pt−Co and Re−Co intereactions by EXAFS. It is possible that the higher Ru loading utilized in this study may have led to a significant number of isolated Ru

particles in addition to those intermixed with Co that could have limited the detection of the interaction by EXAFS. Therefore, additional methods were employed to explore this possibility.

HRTEM images of catalyst RP#1 are shown in Figure 7 (top left and right). Well-defined crystalline structures with characteristic *d*-spacings of 3.3 and 2.0 Å can be seen (top left). The *d*-spacing of 2.0 Å can correspond to the high-intensity [101] plane of hexagonal cobalt phase or the high-intensity [111] plane of the cubic cobalt phase. Similarly, the *d*-spacing of 3.3 Å may be assigned to the [200] plane of hexagonal binary Al/Co mixed oxide. The dark areas (highlighted by white circles) emphasize the presence of heavier elements than Al or Co. These dark areas reveal characteristic *d*-spacings of 2.7 and 2.2 Å, which do not correspond to any crystal plane of either the pure Co or Ru phases. These dark areas might correspond to nanoclusters of Co and/or Co/Ru. The characteristic *d*-spacing for high-intensity [400], [311], and [111] planes of cobalt ruthenium oxide are 2, 2.5, and 4.8 Å. Although the catalysts in the present study were reduced/passivated, some oxidation from the atmosphere during sample preparation and handling for TEM measurements is still possible. In another view (top right), the *d*-spacings of 2.7 and 2.2 Å are observed and may be assigned to the [311] and [400] planes of the Co/Ru binary oxide system. The nanoclusters of heavier atoms are clearly visible. The average diameter of such clusters is in the range 2−3 nm. The HRTEM images of catalysts RP#3 and RP#4 are presented in Figure 7, bottom left and right, respectively. The image for RP#3 (bottom left) reveals the appearance of well-mixed crystalline nanocluster structures and the average diameter (highlighted by a white circle) is in the range 5−10 nm. The darker area highlighted by a white circle has a characteristic *d*-spacing of 4.83 Å which may be assigned to the high-intensity [111] plane of Co/Ru binary mixed oxide. The bottom right image indicates that the average size of nanoclusters in catalyst RP#4 is approximately 20 nm.

The elemental compositions of these nanoclusters were determined by EDS measurements. Relative intensities of Co Kα and Ru Lα lines were used to prepare the quantitative compositional maps of these elements. The quantitative elemental composition maps for catalysts RP#2, RP#3, and RP#4 are shown in Figure 8, parts A, B, and C, respectively. The Co and Ru clusters in RP#2 appear in large part to be quite isolated from one another. However, some mixing, at least on the nanoscale, can be readily observed in sample RP#3 after two oxidation−reduction cycles. In sample RP#4, after three oxidation−reduction cycles, it is clear that even better mixing of the two elements has taken place. It is not clear from the images, however, whether the mixing takes place on the nanoscale (i.e., fusing of nanoclusters of Ru and Co) or on the atomic scale (i.e., alloying). HRTEM images of some of the samples in the present study have shown the appearance of regions which appear as either dark or white spots (depending on the composition). Point/area EDS measurements were utilized to estimate the chemical composition of such spots. Area EDS measurements of such nanoclusters observed in sample RP#4 are shown in Figure 9. The elemental composition of a such a white nanocluster (having a visible difference from the background) was found to be a well-mixed phase of Ru (ca. 1 wt %) and Co (ca. 15 wt %). This result suggests that oxidation−reduction cycles may promote the growth of Co nanoclusters and the formation of a Co−Ru mixed phase. However, again, it is not clear from the EDS scans whether the mixing occurs on the atomic scale (i.e., alloying), nanoscale (i.e., fused domains), or both levels.

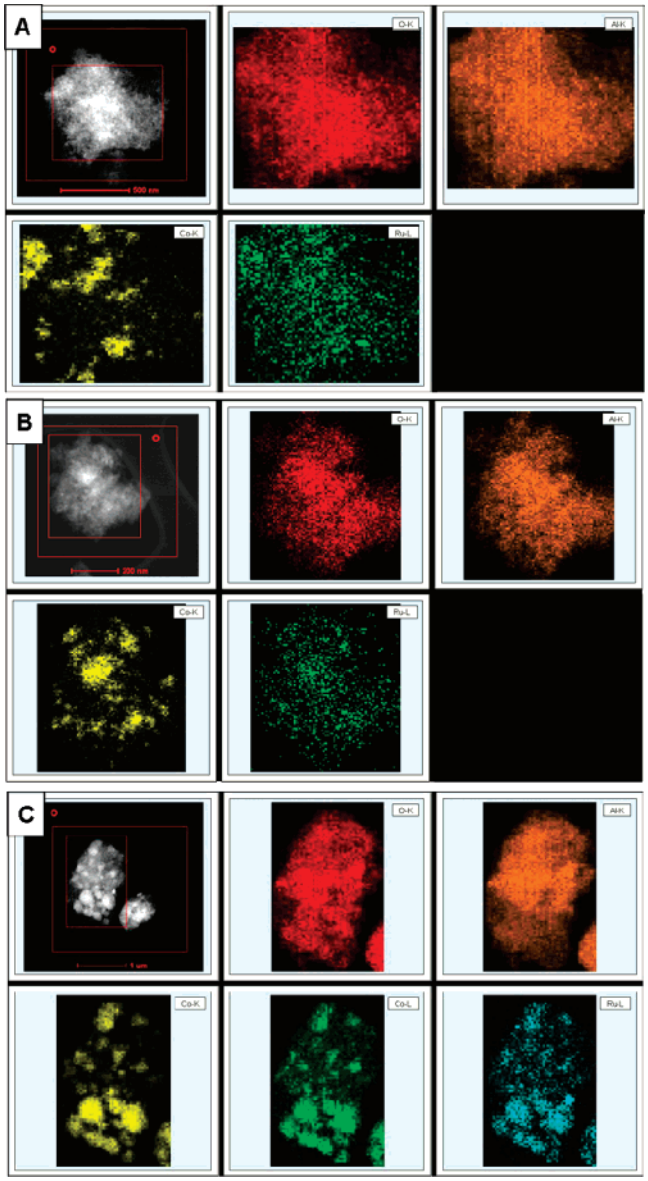

Figure 8. Quantitative elemental composition maps for (A) sample RP#2, (B) sample RP#3, and (C) sample RP#4. The inner red square indicates the area of measurements, while the outer red square shows the corrected area limit. The red dot indicates the point used for "parking" the focused electron beam between EDS recording and area correction.

With a syngas space velocity of 8 sl/h/g of catalyst, the initial activity of the reduced freshly calcined catalyst (a CO conversion level of 37.7%) was found to be higher than that of RP#3 (a CO conversion level of 34.3%). The variation of conversion levels of syngas, CO, and hydrogen against synthesis time for both catalysts are shown in Figures 10 and 11, respectively. The rate of deactivation (expressed in terms of decrease in percent CO conversion per week), rewax selectivity (expressed in terms of grams of rewax produced per day per gram of catalyst), and α-values (calculated by considering a carbon number range of 30−60) for the two catalysts are presented in Table 4. It is evident that, at high syngas SV, the rate of deactivation of the reduced freshly calcined catalyst was higher than that of catalyst RP#3 by a factor of more than 2. When the SV was changed to 3 sl/h/g of catalyst, the activity of RP#3 catalyst (a CO conversion of 58.5%) was found to be higher than that of the reduced freshly calcined catalyst (a CO conversion level of 56.7). However, the rate of deactivation of the freshly calcined catalyst was marginally higher (ca. 5.7%

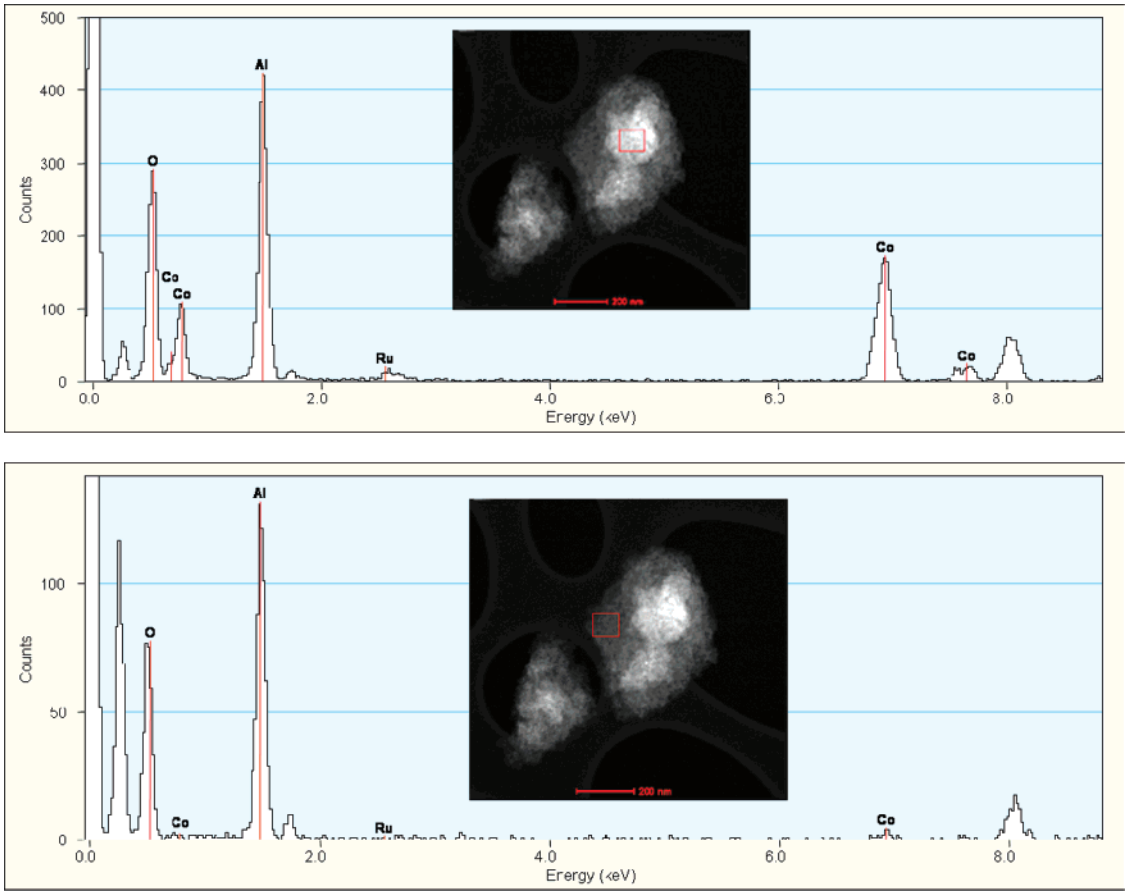

Figure 9. Quantitative EDS elemental point/area composition for sample RP#4. High-resolution STEM images are shown in insets. The red square indicates the area where the electron beam was focused for recording the EDS spectrum.

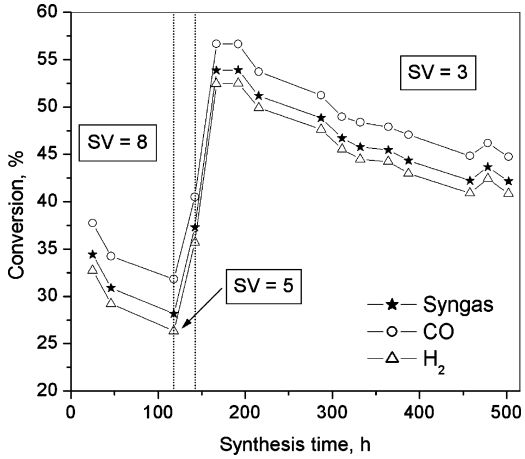

Figure 10. Conversion of syngas, hydrogen, and CO against time-on-stream for the reduced freshly calcined catalyst. FTS effected at 220 °C, 280 psig, $H_2/CO = 2.0$, and an initial syngas space velocity of 8.0 sl/h/g of Fe. After 118 h of synthesis, the syngas SV was lowered to 5 sl/h/g of catalyst, and after 142.25 h, the SV was further changed to 3 sl/h/g of catalyst, which remained unchanged for the rest of the synthesis time.

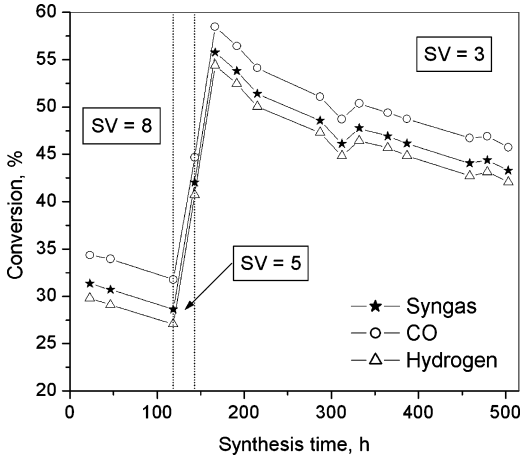

Figure 11. Conversion of syngas, hydrogen, and CO against time-on-stream for catalyst RP#3. FTS effected at 220 °C, 280 psig, $H_2/CO = 2.0$, and an initial syngas space velocity of 8.0 sl/h/g of Fe. After 118.5 h of synthesis, the syngas SV was lowered to 5 sl/h/g of catalyst, and after 143.15 h, the SV was further changed to 3 sl/h/g of catalyst, which remained unchanged for the rest of the synthesis time.

CO conversion decrease per week) than that of catalyst RP#3 (ca. 6% CO conversion decrease per week). The rate of rewax production based on hundreds of grams of wax collected during testing for catalyst RP#3 was found to be higher than that of the reduced freshly calcined catalyst, and in line with this, the α-value for catalyst RP#3 was also higher.

It is important to note that, based on many tests over supported Co catalysts carried out at the Center for Applied Energy Research, the α-value of the wax produced is generally close to 0.87. The higher α-values of 0.90 and 0.92 obtained for the reduced freshly calcined catalyst and RP#3 strongly suggest that Ru itself is participating in the FTS, since it is known to produce very high α-value product. The differences between the two values obtained over the current catalysts likely reflect the resulting Ru/Co surface ratio.

C_{5+} selectivity is an important measure for commercial catalyst operation. A comparison of C_{5+} selectivity (calculated on a carbon atom basis) against synthesis time for both catalysts is presented in Figure 12. Since the on-stream time changes in syngas SV for both reaction tests were identical, a direct

Table 4. Comparison of Catalytic Performances of the Reduced Freshly Calcined Catalyst and RP#3 during FTS at 220 °C 280 psig, H_2/CO = 2.0

catalyst	deactivation rate (% CO conversion/week) at a SV of 8 sl/h/g of catalyst)	deactivation rate (% CO conversion/week) at a SV of 3 sl/h/g of catalyst)	rewax selectivity, g/g of catalyst/day	α ($C_{30}-C_{60}$)
10 h reduced, freshly calcined catalyst	10.65	6.09	1.339	0.902
RP#3	4.546	5.68	2.369	0.919

comparison can be made. The C_{5+} selectivity of catalyst RP#3 was always found to be higher (about 2%) than that of the reduced freshly calcined catalyst for any particular SV of syngas. This result suggests that more carbon atoms in the feed were converted to useful Fischer−Tropsch synthesis (FTS) products (i.e., oil, wax, and rewax fractions) by catalyst RP#3 relative to the reduced freshly calcined catalyst. A comparison of methane selectivity data between the two catalysts shown in Figure 13 reveals that catalyst RP#3 exhibited lower methane selectivity than the reduced freshly calcined catalyst.

The above results indicate that catalyst RP#3 has higher stability, and higher C_{5+} selectivity, compared to the reduced freshly calcined catalyst. In a Fischer−Tropsch operation where rewax is the desired product, catalyst RP#3 will be a better choice than using a freshly calcined catalyst. Since both catalysts have the same composition, the results reveal that the higher stability and higher rewax selectivity was promoted by the structural changes induced by the oxidation−reduction cycle treatments of the catalyst. The oxidation−reduction cycles have aided the growth of the cobalt nanoclusters to a more robust size, while reduction of the freshly calcined catalyst led to a correspondingly smaller size. Based on the results of this investigation, the moderately sized cobalt nanocluster appears to reflect a careful balance between the number of cobalt metal surface atoms available for FTS and a higher catalytic stability due to its larger size, which makes it less prone to sintering and cobalt−support complex formation. In addition, the cobalt in the catalysts subjected to the oxidation−reduction cycles exhibit enhanced reducibility due to at least two factors: (1) there is an improvement in the cobalt−ruthenium promoter interaction and (2) the larger cluster size weakens the interaction with the alumina support.

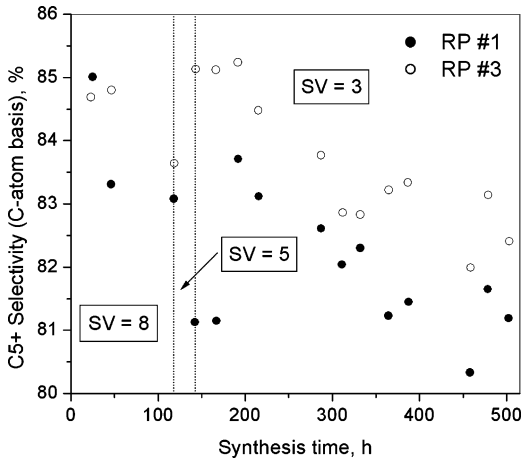

Figure 12. Comparison of C_{5+} selectivity (on a carbon atom basis) against time-on-stream (TOS) for the reduced freshly calcined catalyst and RP#3. The syngas space velocities for both of the runs were changed about same time: 8.0 sl/h/g of Fe to 5 sl/h/g of catalyst about 118 h of TOS and 5 sl/h/g of catalyst to 3 sl/h/g about 143 h of TOS.

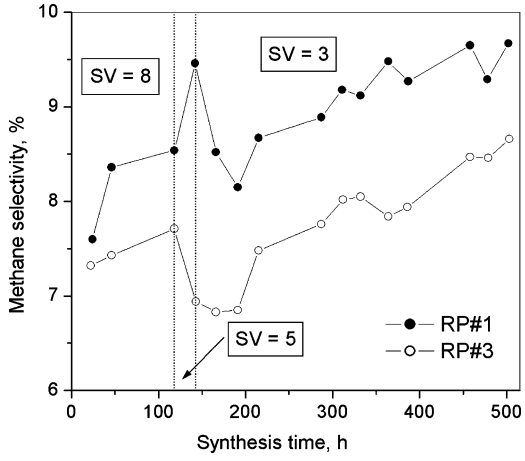

Figure 13. Comparison of methane selectivity (on a carbon atom basis) against time-on-stream for the reduced freshly calcined catalyst and catalyst RP#3. The syngas space velocities for both of the runs were changed about same time: 8.0 sl/h/g of Fe to 5 sl/h/g of catalyst about 118 h of TOS and 5 sl/h/g of catalyst to 3 sl/h/g about 143 h of TOS.

4. Conclusions

EXAFS and HRTEM data indicated that the oxidation−reduction treatments were found to assist in sintering the metallic clusters to a larger size, while EDS elemental mapping showed that the oxidation−reduction treatments promoted mixing of Co and Ru on at least the order of the nanoscale. The larger crystallites in closer proximity to the Ru promoter led to a more facile reduction of the cobalt crystallites, as clearly indicated by XANES, EXAFS, and TPR measurements. In reaction testing, the catalyst exposed to two oxidation−reduction cycles resulted in slightly higher conversion, higher α-value product, slightly lower methane selectivity, and greater stability versus a reduced freshly calcined catalyst. Based on the α-values, it appears that at least part of the Ru is acting alone in the FTS to produce products with an α-value considerably higher than the 0.87 normally associated with Co, or the Co−Ru alloy behaves more like Ru than Co.

Acknowledgment

The work was supported by the Commonwealth of Kentucky. This research was carried out, in part, at the National Synchrotron Light Source (NSLS), Brookhaven National Laboratory (BNL), which is supported by the U.S. Department of Energy, Division of Materials Science and Chemical Sciences. We express special thanks to Dr. Syed Khalid (Beamline X18b, NSLS, Brookhaven) for help with XAFS studies and Joel Young (Department of Physics, University of Oklahoma) for XAFS cell construction. Research carried out (in part) at the NSLS, at BNL, is supported by the U.S. Department of Energy, Division of Materials Science and Division of Chemical Sciences, under Contract No. DE-AC02-98CH10886.

Literature Cited

(1) van Berge; P. J.; Barradas, S.; van de Loosdrecht, J.; Visagie, J. Advances in the cobalt catalyzed Fischler-Tropsch synthesis. *Erdoel, Erdgas, Kohle* **2001**, *117*, 138.

(2) van Berge, P. J.; van de Loosdrecht, J.; Barradas, S.; van der Kraan, S. A. M. Oxidation of cobalt based Fischer-Tropsch catalysts as a deactivation mechanism. *Catal. Today* **2000**, *58*, 321.

(3) Jacobs, G.; Das, T. K.; Zhang, Y.; Li, J.; Racoillet, G.; Davis, B. H. Fischer-Tropsch synthesis: support, loading and promoter effects on the reducibility of cobalt catalysts. *Appl. Catal., A* **2002**, *233*, 281.

(4) Saib, A. M.; Borgna, A.; van de Loosdrecht, J.; van Berge, P. J.; Niemantsverdriet, J. W. XANES study of the susceptibility of nano-sized cobalt crystallites to oxidation during realistic Fischer-Tropsch synthesis. *Appl. Catal., A* **2006**, *312*, 12.

(5) Bertole, C. J.; Mims, C. A.; Kiss, G. The effect of water on the cobalt-catalyzed Fischer-Tropsch synthesis. *J. Catal.* **2002**, *210*, 84.

(6) Jacobs, G.; Patterson, P. M.; Zhang, Y.; Das, T. K.; Li, J.; Davis, B. H. Fischer-Tropsch synthesis: deactivation of noble metal-promoted Co/Al_2O_3 catalysts. *Appl. Catal., A* **2002**, *233*, 215.

(7) Das, T. K.; Jacobs, G.; Patterson, P. M.; Conner, W. A.; Li, J.; Davis, B. H. Fischer-Tropsch synthesis: characterization and catalytic properties of rhenium promoted cobalt alumina catalysts. *Fuel* **2003**, *82*, 805.

(8) Schanke, D.; Hilmen, A. M.; Bergene, E.; Kinnari, K.; Rytter, E.; Adnanes, E.; Holmen, A. Study of the deactivation mechanism of Al_2O_3-supported cobalt Fischer-Trospch catalysts. *Catal. Lett.* **1995**, *34*, 269.

(9) Hilmen, A. M.; Schanke, D.; Hanssen, K.; Holmen, A. Study of the effect of water on alumina supported cobalt Fischer-Tropsch catalysts. *Appl. Catal., A* **1999**, *186*, 169.

(10) Li, J.; Zhan, X.; Zhang, Y.; Jacobs, G.; Das, T. K.; Davis, B. H. Fischer-Tropsch synthesis: effect of water on the deactivation of Pt promoted Co/Al_2O_3 catalysts. *Appl. Catal., A* **2002**, *228*, 203.

(11) Jacobs, G.; Das, T. K.; Patterson, P. M.; Li, J.; Sanchez, L.; Davis, B. H. Fischer-Tropsch synthesis XAFS: XAFS studies of the effect of water on a Pt-promoted Co/Al_2O_3 catalyst. *Appl. Catal., A* **2003**, *247*, 335.

(12) Jacobs, G.; Patterson, P. M.; Das, T. K.; Luo, M.; Davis, B. H. Fischer-Tropsch synthesis: effect of water on Co/Al_2O_3 catalysts and XAFS characterization of reoxidation phenomena. *Appl. Catal., A* **2004**, *270*, 65.

(13) Storsaeter, S.; Borg, O.; Blekkan, E. A.; Holmen, A. Study of the effect of water on Fischer-Tropsch synthesis over supported cobalt catalysts. *J. Catal.* **2005**, *231*, 405.

(14) Zhang, Y.; Wei, D.; Hammache, S.; Goodwin, J. G., Jr. Effect of water vapor on the reduction of Ru-promoted Co/Al_2O_3. *J. Catal.* **1999**, *188*, 281.

(15) Jongsomjit, B.; Panpranot, J.; Goodwin, J. G., Jr. Co-support compound formation in alumina-supported cobalt catalysts. *J. Catal.* **2001**, *204*, 98.

(16) Sirijaruphan, A.; Horvath, A.; Goodwin, J. G., Jr.; Oukaci, R. Cobalt aluminate formation in alumina-supported cobalt catalysts: effects of cobalt reduction state and water vapor. *Catal. Lett.* **2003**, *91*, 89.

(17) Bartholomew, C. H.; Zennaro, R.; Huber, G. W. Kinetics of Fischer-Tropsch synthesis on titania- and silica-supported cobalt. Presented at the 217th National Meeting of the American Chemical Society, Anaheim, CA, March 21−25, 1999.

(18) Krishnamoorthy, S.; Tu, M.; Ojeda, M. P.; Pinna, D.; Iglesia, E. An investigation of the effects of water on rate and selectivity for the Fischer-Tropsch synthesis on cobalt-based catalysts. *J. Catal.* **2002**, *211*, 422.

(19) Bezemer, G.; Leendert, G.; Bitter, J. H.; Kuipers, H. P. C. E.; Oosterbeek, H.; Holewijn, J. E.; Xu, X.; Kapteijn, F.; van Dillen, A. J.; de Jong, K. P. Cobalt particle size effects in the Fischer-Tropsch reaction studied with carbon nanofiber supported catalysts. *J. Am. Chem. Soc.* **2006**, *128*, 3956.

(20) Dalai, A. K.; Das, T. K.; Chaudhari, K. V.; Jacobs, G.; Davis, B. H. Fischer-Tropsch synthesis: water effects on Co supported on narrow and wide-pore silica. *Appl. Catal., A* **2005**, *289*, 135.

(21) Iglesia, E. Design, synthesis and use of cobalt-based Fischer-Tropsch synthesis catalysts. *Appl. Catal., A* **1997**, *161*, 59.

(22) Ressler, T. *WinXAS 97*, version 1.0; 1997.

(23) Ravel, B. EXAFS analysis using FEFF and FEFFIT workshop, June 27, 2001.

(24) Newville, M.; Ravel, B.; Haskel, D.; Stern, E. A.; Yacoby, Y. Analysis of multiple-scattering XAFS data using theoretical standards. *Physica B* **1995**, *154*, 208−209.

Received for review July 23, 2007
Revised manuscript received September 26, 2007
Accepted October 26, 2007

IE0709988